DOI 10.1002/dneu.22137

Altered expression of atypical PKC and Ryk in the spinal cord of a mouse model of amyotrophic lateral sclerosis

Anna Tury, Kristine Tolentino and Yimin Zou*

University of California, San Diego, Division of Biological Sciences, Section of Neurobiology, 9500 Gilman Drive, La Jolla, CA 92093, USA.

***Corresponding author**: Yimin Zou, University of California, San Diego, Division of Biological Sciences, Section of Neurobiology, La Jolla, CA, USA. E-mail: yzou@ucsd.edu. Phone: 858-534-7212. Fax: 858-534-6512

Running title: aPKC and Ryk in ALS

Five key words: aPKC, Ryk, neurodegeneration, ALS, SOD1 (G93A)

Number of figures: 6

Acknowledgments:

We thank Lucia Chen and Rebecca McRae for their help for tissue processing and immunohistochemistry.

Source of funding: Packard Center, NIH RO1 (NS 047484)

Received: Jul 01, 2013; Revised: Sep 24, 2013; Accepted: Sep 25, 2013

ABSTRACT

Amyotrophic lateral sclerosis (ALS) is a fatal neurodegenerative disease characterized by progressive paralysis due to the selective death of motor neurons of unknown causes. Increasing evidence indicates that Wnt signaling is altered in ALS. In this study, we focused on two non-canonical Wnt signaling components, atypical PKC (aPKC) and a Wnt receptor, Ryk, in a mouse model of ALS, SOD1 (G93A). aPKC mediates Wnt signaling to regulate growth cone guidance, axon differentiation and cell survival. Ryk is a Wnt repulsive receptor that regulates axon guidance and inhibits regeneration after spinal cord injury. aPKC expression was increased in motor neurons of the lumbar spinal cord in SOD1 (G93A) mice at different stages. Interestingly, aPKC was colocalized with SOD1 in motor neuron cell bodies and extracellular aggregates, and aPKC-containing extracellular aggregates increased with disease progression. Biochemical fractionation showed that aPKC protein level was increased in the detergent-insoluble protein fraction in SOD1 (G93A) mice at late stage but decreased in the detergent-soluble fraction at symptomatic stage. These results suggest that aPKC may be sequestered in SOD1 aggregates, impairing its ability to protect motor neurons from death. Ryk expression was also increased in the motor neurons and the white matter in the ventral lumbar spinal cord of mutant SOD1 mice with a peak at early stage. These observations indicate that Wnt/aPKC and Wnt/Ryk signaling are altered in SOD1 (G93A) mice, suggesting that changed Wnt signaling may contribute to neurodegeneration in ALS.

INTRODUCTION

Amyotrophic lateral sclerosis (ALS) is a neurodegenerative disease of motor neurons with no effective treatment (Cleveland and Rothstein, 2001; Bruijn et al., 2004; Pasinelli and Brown, 2006; Pratt et al., 2012). Genetic studies identified mutations in several genes including superoxide dismutase 1 (SOD1), ataxin-2, TDP-43, Fus and C9ORF72 (Pratt et al., 2012). How these mutations cause ALS is still not known. One approach to understand pathogenesis of ALS is to investigate how these mutations affect the normal signaling pathways that regulate neuronal survival and degeneration.

Wnt signaling plays important roles in nervous system development and function, including axon guidance, synapse formation and plasticity (Zou, 2004; Salinas and Zou, 2008) and has also been associated with neurodegenerative diseases, including Alzheimer disease, Parkinson disease, frontotemporal dementia and ALS (De Ferrari and Inestrosa, 2000; Nusse, 2005; Inestrosa and Toledo, 2008; Rosen et al., 2011; Berwick and Harvey, 2012; Chen et al., 2012a; Chen et al., 2012b). Axon degeneration is an important step in disease progression, although the key regulators are not well characterized in degenerative disorders. We found previously that atypical PKC (aPKC) mediates axon attraction to Wnts and anterior-posterior axon guidance (Wolf et al., 2008). In cultured hippocampal neurons, aPKC was also shown regulated by disheveled (Dvl) in axon determination during neuronal polarization (Zhang et al., 2007). Interestingly, aPKC was reported to promote survival in many cell types including neurons (Wooten, 1999; Wooten et al., 2000; Xie et al., 2000; Huang et al., 2001; Xin et al., 2007). However, recently it was shown to have proapoptotic function in ovarian cancer (Nazarenko et al., 2010). Ryk is a Wnt binding receptor that mediates axon repulsion in development and inhibition of axon plasticity in adulthood after traumatic injury (Liu et al., 2005; Keeble and Cooper, 2006; Keeble et al., 2006; Schmitt et al., 2006) (Liu et al., 2008; Miyashita

et al., 2009; Fradkin et al., 2010; Hollis and Zou, 2012b; Hollis and Zou, 2012a; Gonzalez et al., 2013). Therefore, we elected to characterize these two key regulators of axon growth and plasticity in animal models of ALS.

Familial ALS accounts for 5-10% of ALS cases. Approximately 20% of inherited cases of ALS are caused by mutations in SOD1 gene, one of the first ALS genes (Rosen, 1993; Valentine et al., 2005; Mulligan and Chakrabartty, 2013). Overexpression of mutant forms of human SOD1 such as SOD1 (G93A) in transgenic mice mimics human ALS disease symptoms and progression (Gurney et al., 1994; Peviani et al., 2010). To date, SOD1 (G93A) is one of the better-characterized mouse models of ALS.

We examined expression patterns and levels of aPKC and Ryk in the lumbar spinal cord of SOD1 (G93A) mouse. We found that aPKC was up regulated in motor neurons at all stages of disease progression (postnatal day 30 (P30) to P120). Interestingly, aPKC was also detected in extracellular SOD1 aggregates, and aPKC extracellular aggregates increased with disease progression. Using biochemical fractionation, we then found that aPKC was enriched in detergent-insoluble fraction at late stage and the level of activated aPKC in the soluble fraction was greatly reduced at symptomatic stage. Ryk was also increased in motor neuron cell bodies and motor axons of the ventral white matter of ALS mice from P30 to P120, with a peak of increase at early stage. Therefore, the expression of the two key regulators of axon growth and plasticity are drastically altered in a mouse model of ALS.

METHODS

Animals

SOD1 (G93A) (B6SJL-Tg(SOD1-G93A)1Gur/J #002726), SOD1 (WT) (B6SJL-Tg(SOD1)2Gur/J #002297) and B6SJLF1/J (#100012) mice were purchased from The Jackson Laboratory (Sacramento, CA). Male mice hemizygous for SOD1 (G93A) or SOD1 (WT) were crossed with female F1 hybrid B6SJLF1/J mice. Animals were housed in a temperature-controlled room with standard laboratory food and water provided *ad libitum*. All animal manipulations and experimental procedures were performed in accordance with the animal experimentation guidelines of our institution, IACUC and NIH.

Antibodies

Primary antibodies used in this study included P-PKCζ T410 (Santa Cruz Biotechnology, Santa-Cruz, CA, sc-101778, rabbit, 1:1000 for Western-blotting), total PKCζ (Santa Cruz Biotechnology, C-20 sc-216, rabbit, 1:100 for immunohistochemistry, 1:2000 for Western-blotting), P- PKCζ T410 (Santa Cruz Biotechnology, sc-101778, rabbit,1:1000 for Western-blotting), Ryk ((Liu et al., 2005), Rabbit 1:100 for immunohistochemistry), Choline acetyltransferase (ChAT, Millipore, Billerica, MA, goat, 1:100 for immunohistochemistry), glial fibillary acidic protein (GFAP, Dako, Carpinteria, CA, mouse, 1:1000 for immunohistochemistry), Neurofilament-200 (Sigma, St-Louis, MO, mouse, 1:1000 for immunohistochemistry), SMI-312 (Covance, San Diego, CA, mouse, 1:1000), CC1 (Millipore, mouse, 1:200 for immunohistochemistry), rabbit SOD1 (Genetex, Irvine, CA, 1:2000 for Western-blotting and 1:500 immunohistochemistry), mouse SOD1 (OriGene, 1:200 for immunohistochemistry) and GAPDH (Millipore, mouse, 1:50,000 for Western-blotting).

Tissue processing and Immunohistochemistry

Mice were deeply anesthetized with a mix of ketamine/xylasine and transcardially perfused with ice-cold phosphate buffer saline (PBS) followed by ice-cold 4% paraformaldehyde in PBS. Spinal cords were dissected and post-fixed in the same fixative for 2h at 4ºC and immersed in 30% sucrose in PBS overnight at 4ºC for cryoprotection. Spinal cords were cut into three segments: cervical, thoracic and lumbar. The lumbar segments of the spinal cords were embedded in a commercial embedding medium (Tissue-Tek, Sakura Finetek, Torrance, CA), quickly frozen on dry-ice and coronally sectioned at a thickness of 14 µm using a cryostat-microtome (Leica, Buffalo Grove, IL). Sections were mounted on Superfrost Plus slides (Thermo Fisher Scientific, Pittsburgh, PA) and stored at -20ºC. Sections were rinsed in PBS containing 0.3% triton X-100 (PBS-T) for 10 min and incubated with the primary antibody overnight at 4ºC. Antibodies were diluted in a PBS-T blocking solution containing 10% lactoproteins and 1% bovine serum albumin. Staining was visualized using Alexa Fluor 488, 594 or 649 conjugated secondary antibodies (Jackson ImmunoReasearch, West Grove, PA, 1:500). Sections were counterstained with 4'-6-diamidino-2-phenylindole (DAPI) (Thermo Fisher Scientific).

Protein extraction and Western-blotting

Detergent-soluble and -insoluble protein fractions were obtained as previously described with some modifications (Dammer et al., 2012). Briefly, the lumbar segments of the spinal cords were dissected and homogenized in lysis buffer 1 containing 20 µM Tris-HCl pH 7.6, 150 µM NaCl, 0.1% SDS, 1% triton X-100, protease inhibitors (Complete mini tablets, Roche Applied Science, Indianapolis, IN) and phosphatase inhibitors (PhosSTOP, Roche Applied Science). After 30 min incubation on ice, lysates were centrifuged at 13,000g for 30 min at 4ºC to generate the detergent-soluble supernatants and insoluble pellets. Detergent-insoluble pellets were washed twice with lysis buffer 1, resuspended in lysis buffer 2 containing 6M urea, 2% SDS, benzonase (250U/ml) and protease inhibitors, and sonicated (10s, 3 times). After 30 min incubation on ice, lysates were centrifuged at 13,000 g for 30 min at 4ºC and the supernatants

were saved as the detergent-insoluble fractions. Protein concentrations were determined using the Bio-Rad protein assay (Bio-Rad, Hercules, CA). Twenty-five micrograms of proteins were separated by SDS PAGE and then electro-transferred onto polyvinylidene difluoride membranes (Bio-Rad). Membranes were blocked with blocking buffer containing 2% BSA or 5% fat-free dry milk in Tris-buffered saline solution and Tween 20 (10 mM Tris-HCl pH 7.4, 150 mM NaCl, 0.05% Tween 20) and incubated overnight at 4°C with primary antibody diluted in blocking buffer. Incubations with HRP conjugated secondary antibodies (1:5000) were performed for 1h at room temperature and visualization was performed using chemiluminescence (Thermo Fisher Scientific).

Image acquisition and analysis

Images were acquired on an inverted Zeiss LSM510 confocal microscope with LSM acquisition software (Carl Zeiss Microscopy, LLC, Thornwood, NY) using the Z-stack function with a conserved interval. Exposure time was adjusted to be under the saturation level for the highest immunofluorescence signal and was conserved between the different samples. Measurements of mean immunofluorescence intensity level in the motor neuron cell bodies of the ventral spinal cord were performed on Z-projected images with maximum intensity using FiJi-ImageJ software (NIH, Bethesda, MD). Measurement of pixel density of Ryk immunofluorescence in the white matter of the lumbar ventral spinal cord was done on thresholded fluorescent images. Left and right horns of the ventral spinal cord were analyzed on 3 sections per animal. The number of animals analyzed for aPKC and Ryk expression quantification in motor neurons were as follow: P30: NT: n=8, SOD1-WT: n=4, SOD1-G93A n=7; P60: NT: n=7, SOD1-WT: n=3, SOD1-G93A n=7; P90: NT: n=3, SOD1-WT: n=6, SOD1-G93A n=4; P120: NT: n=5, SOD1-WT: n=6, SOD1-G93A n=10.

Statistical analysis

Statistical analyses were performed using ANOVA with Bonferroni Post-test or Student's t test using GraphPad Instat 3.05 (GraphPad Software). All data are expressed as means or percents±s.e.m. *p<0.05, **p<0.01, ***p<0.001.

RESULTS

aPKC and Ryk are expressed in adult motor neurons and oligodendrocytes but not in astrocytes

We first determined the expression patterns of aPKC and Ryk in the ventral horn of the lumbar segment of normal adult mouse spinal cords by immunohistochemistry, using antibodies that were previously characterized (Liu et al., 2005; Guenther et al., 2012). To label cell types, we used the following markers, NF-200 which labels the neurofilament heavy subunits in neurons, ChAT for cholinergic motor neurons, GFAP for astrocytes and CC1 for mature oligodendrocytes. The aPKC antibody recognizes all isoforms of aPKC family, PKCζ, PKCλ/i and PKMζ. We found that aPKC was expressed in motor neurons labeled with NF-200 and ChAT as well as in smaller ChAT-negative neurons (Fig. 1A). aPKC was not expressed in $GFAP^+$ astrocytes (Fig. 1B) but was expressed in mature oligodendrocytes labeled with CC1 in the white matter (Fig. 1C). A small number of $aPKC^+$ $CC1^+$ cells were also detected in the grey matter of the ventral horn (Fig. 1C). aPKC immunoreactivity was mostly localized on cell bodies, both in the cytoplasm and nucleus (Fig. 1D). Ryk was found expressed in the cytoplasm of the cell bodies and in fibers of $NF\text{-}200^+$ $ChAT^+$ motor neurons (Fig. 1E,H). Similar to aPKC, Ryk was not detected in $GFAP^+$ astrocytes (Fig. 1F) but was detected in scattered $CC1^+$ oligodendrocytes in the ventral white and grey matter (Fig. 1G). Ryk was also detected in some $ChAT^+$ motor axons in the ventral white matter (Fig. 1E).

aPKC expression is increased in motor neurons in the lumbar spinal cord of SOD1 (G93A) mice

Symptom progression in SOD1 (G93A) mouse model is divided into four stages: early stage (P30), pre-symptomatic stage (P60), symptomatic stage (P90) and end stage (P120). We found that aPKC immunoreactivity was increased in $ChAT^+$ motor neuron cell bodies in SOD1 (G93A) lumbar spinal cords at all stages (Fig. 2A,B). aPKC immunoreactivity also showed a mild trend of increase in motor neurons of SOD1 (WT) mice compare to non transgenic mice but the difference was not statistically significant (Fig. 2A,B). As expected in this mouse model, the number of $ChAT^+$ motor neurons was decreased in the lumbar spinal cord of SOD1 (G93A) at P90 and P120 but not at earlier stages (Fig. 2C). However, the level of aPKC expression in motor neurons did not gradually increase with the symptom progression, the peak being greater at early stage. (Fig. 2A,B).

aPKC colocalizes with SOD1 extracellular aggregates

To better characterize the localization of aPKC, we performed double immunostaining with a human SOD1 antibody. We found that aPKC colocalized with human SOD1 protein in both motor neuron cell bodies and extracellular SOD1 aggregates in the ventral horn of the spinal cord of SOD1 (G93A) at P120 (Fig. 3A,B). Furthermore, aPKC extracellular aggregates increased with symptom progression (Fig. 3C). Using biochemical fractionation, we found that aPKC protein level increased in the detergent-insoluble fraction in P120 SOD1 (G93A) lumbar spinal cord (Fig. 4A). Consistent with this, we found that aPKC activity decreased in the detergent-soluble fraction in the lumbar spinal cord of SOD1 (G93A) mice as shown by the reduction of phosphorylation of PKCζ-T410 at P90 (Fig. 4B). Total PKCζ protein level was also decreased at P90 (Fig. 4B), suggesting that aPKC protein stability decreases when its activity is

reduced. A similar trend, but not statistically significant, of decrease of PKCζ phosphorylation was observed at P30 with no change in total PKCζ protein level (Fig. 4B).

Ryk expression is increased in the motor neurons and the ventral white mater in the lumbar spinal cord of SOD1 (G93A) mice

We performed immunostaining with our Ryk antibodies in the lumbar spinal cord of SOD1 (G93A) mice at different stages (Liu et al 2005). We found that Ryk immunoreactivity was increased in the cell bodies of $ChAT^+$ motor neurons at all stages with a peak at P30 (Fig. 5A,B). Ryk immunoreactivity was also increased in the ventral white mater (Fig. 5C,D) and colocalized with NF-200 (Fig. 5E), suggesting that Ryk is expressed and increased in motor neuron axons. To confirm that, we used a pan-axonal neurofilament marker, SMI-312, and found that Ryk was colocalized with SMI-312 in motor axons of the ventral roots (Fig. 5F).

Ryk colocalizes with human SOD1 protein but not in the extracellular SOD1 deposits

To better characterize the localization of Ryk, we performed double immunostaining with human SOD1 antibody. We found that Ryk colocalized with human SOD1 protein in $ChAT^+$ motor neurons in the grey matter (Fig. 6A) and in axons in the ventral white matter (Fig. 6B) in the lumbar spinal cord of SOD1-G93A mice. However, contrary to aPKC, Ryk protein was not detected in the extracellular SOD1 deposits found at symptomatic and end stages.

DISCUSSION

The mechanisms underlying motor neuron cell death and axonal degeneration in ALS remain elusive. This is partly due to the fact that the biological mechanisms of neuronal degeneration are not well understood. In this study, we found that two non-canonical Wnt signaling components, aPKC and Ryk, which are important regulators of axon growth and plasticity in both developing embryos and in adult nervous system, were clearly up regulated in the spinal cord of SOD1 (G93A) mice, providing additional evidence that Wnt signaling is altered in ALS and might be involved in disease etiology and pathogenesis (Chen et al., 2012a; Chen et al., 2012b; Wang et al., 2013; Yu et al., 2013). This should inspire more studies on the role of Wnt signaling in ALS.

Our results indicate that aPKC expression was robustly increased in motor neurons in the spinal cord of SOD1 (G93A) mice throughout symptom progression, including early and pre-symptomatic stages before neuronal loss occurs. Our finding is consistent with a report showing that PKCζ protein level was up regulated in the spinal cord of ALS patients and in an SOD1 transgenic model by Western blotting (Hu et al., 2003a; Hu et al., 2003b). The significance of this increase of immunoreactivity is currently unknown. One recent study linked aPKC to a proapoptotic function in ovarian cancer (Nazarenko et al., 2010). If aPKC has similar function in neuron, then this early and sustained up regulation of aPKC might cause motor neuron degeneration. However, more studies actually reported that aPKC plays an anti-apoptotic role in different cell types, including neurons (Wooten, 1999; Wooten et al., 2000; Xie et al., 2000; Huang et al., 2001; Wang et al., 2005; Xin et al., 2007). Furthermore, aPKC was thought to promote spontaneous plasticity and functional recovery following spinal injury (Guenther et al., 2012). Therefore, aPKC up regulation might represent a cellular response to protect motor neurons from mutant SOD1 toxicity. In SOD1 (G93A) mice, we found that aPKC colocalized with SOD1 in motor neurons and extracellular SOD1 aggregates, and that aPKC-containing

extracellular aggregates increased with disease progression, suggesting that aPKC may be sequestered in SOD1 aggregates and not function properly. Indeed, aPKC was enriched in the detergent-insoluble fraction in SOD1 (G93A) mice at late stage but decreased in the detergent soluble fraction at symptomatic stages. Similarly, other groups found PKCζ in aggregates containing limbic neurofibrillary tangles and AMPA receptor in Alzheimer patient brains (Crary et al., 2006). PKCι/λ was also detected in tau-positive neurofibrillary inclusions in a variety of tauopathies, including Alzheimer disease, in alpha-synuclein-positive Lewy bodies in idiopathic Parkinson disease, in Lewy bodies in dementia and in glial inclusions in multisystem atrophy (Shao et al., 2006). Together, these results suggest that association of aPKC with protein aggregation could be a common mechanism in the pathogenesis of many neurodegenerative diseases.

We also report here that the expression of a repulsive Wnt receptor, which causes axon retraction and inhibits axon plasticity, Ryk, was robustly increased in motor neurons and in NF-200^{+} axons of the ventral white matter through all stages of the symptom progression, with a peak at early stage. Altered axon guidance pathways have been proposed to cause loss of connectivity in neurodegenerative disorders (Lesnick et al., 2008; Lin et al., 2009; Vanderhaeghen and Cheng, 2010). Increasing evidence suggests an association between aberrant function or expression of axon guidance proteins, such as Semaphorins, Ephrins, Netrins and Slits, with ALS (Schmidt et al., 2009). An increasing number of studies also indicate that Wnt signaling components such as Wnt3a, β-catenin (Chen et al., 2012a), Wnt2, Wnt7a (Chen et al., 2012b) and Wnt4 (Yu et al., 2013) are altered in ALS. Moreover, a recent study showed that the protein level of Wif, which shares sequence homology with the Wnt binding domain of Ryk, was also up regulated in the spinal cord of SOD1 (G93A) mice (Yu et al., 2013). Therefore, together with our current observation, these findings suggest that dysfunction in Wnt signaling and/or other axon guidance signallng pathways might contribute to the pathogenesis

of ALS. Further studies of their mechanisms mediating axon guidance and plasticity and how the disruption of their functions may contribution to ALS will shed light on the disease mechanisms and provide new therapeutic targets.

REFERENCES

Berwick DC, Harvey K. 2012. The importance of Wnt signalling for neurodegeneration in Parkinson's disease. Biochem Soc Trans 40:1123-1128.

Bruijn LI, Miller TM, Cleveland DW. 2004. Unraveling the mechanisms involved in motor neuron degeneration in ALS. Annu Rev Neurosci 27:723-749.

Chen Y, Guan Y, Liu H, Wu X, Yu L, Wang S, Zhao C, Du H, Wang X. 2012a. Activation of the Wnt/beta-catenin signaling pathway is associated with glial proliferation in the adult spinal cord of ALS transgenic mice. Biochem Biophys Res Commun 420:397-403.

Chen Y, Guan Y, Zhang Z, Liu H, Wang S, Yu L, Wu X, Wang X. 2012b. Wnt signaling pathway is involved in the pathogenesis of amyotrophic lateral sclerosis in adult transgenic mice. Neurol Res 34:390-399.

Cleveland DW, Rothstein JD. 2001. From Charcot to Lou Gehrig: deciphering selective motor neuron death in ALS. Nat Rev Neurosci 2:806-819.

Crary JF, Shao CY, Mirra SS, Hernandez AI, Sacktor TC. 2006. Atypical protein kinase C in neurodegenerative disease I: PKMzeta aggregates with limbic neurofibrillary tangles and AMPA receptors in Alzheimer disease. J Neuropathol Exp Neurol 65:319-326.

Dammer EB, Fallini C, Gozal YM, Duong DM, Rossoll W, Xu P, Lah JJ, Levey AI, Peng J, Bassell GJ, Seyfried NT. 2012. Coaggregation of RNA-binding proteins in a model of TDP-43 proteinopathy with selective RGG motif methylation and a role for RRM1 ubiquitination. PLoS One 7:e38658.

De Ferrari GV, Inestrosa NC. 2000. Wnt signaling function in Alzheimer's disease. Brain Res Brain Res Rev 33:1-12.

Fradkin LG, Dura JM, Noordermeer JN. 2010. Ryks: new partners for Wnts in the developing and regenerating nervous system. Trends Neurosci 33:84-92.

Gonzalez P, Fernandez-Martos CM, Arenas E, Rodriguez FJ. 2013. The ryk receptor is expressed in glial and fibronectin-expressing cells after spinal cord injury. J Neurotrauma 30:806-817.

Guenther CH, Windelborn JA, Tubon TC, Jr., Yin JC, Mitchell GS. 2012. Increased atypical PKC expression and activity in the phrenic motor nucleus following cervical spinal injury. Exp Neurol 234:513-520.

Gurney ME, Pu H, Chiu AY, Dal Canto MC, Polchow CY, Alexander DD, Caliendo J, Hentati A, Kwon YW, Deng HX, et al. 1994. Motor neuron degeneration in mice that express a human Cu,Zn superoxide dismutase mutation. Science 264:1772-1775.

Hollis ER, 2nd, Zou Y. 2012a. Expression of the Wnt signaling system in central nervous system axon guidance and regeneration. Front Mol Neurosci 5:5.

Hollis ER, 2nd, Zou Y. 2012b. Reinduced Wnt signaling limits regenerative potential of sensory axons in the spinal cord following conditioning lesion. Proc Natl Acad Sci U S A 109:14663-14668.

Hu JH, Chernoff K, Pelech S, Krieger C. 2003a. Protein kinase and protein phosphatase expression in the central nervous system of G93A mSOD over-expressing mice. J Neurochem 85:422-431.

Hu JH, Zhang H, Wagey R, Krieger C, Pelech SL. 2003b. Protein kinase and protein phosphatase expression in amyotrophic lateral sclerosis spinal cord. J Neurochem 85:432-442.

Huang NK, Lin YW, Huang CL, Messing RO, Chern Y. 2001. Activation of protein kinase A and atypical protein kinase C by A(2A) adenosine receptors antagonizes apoptosis due to serum deprivation in PC12 cells. J Biol Chem 276:13838-13846.

Inestrosa NC, Toledo EM. 2008. The role of Wnt signaling in neuronal dysfunction in Alzheimer's Disease. Mol Neurodegener 3:9.

Keeble TR, Cooper HM. 2006. Ryk: a novel Wnt receptor regulating axon pathfinding. Int J Biochem Cell Biol 38:2011-2017.

Keeble TR, Halford MM, Seaman C, Kee N, Macheda M, Anderson RB, Stacker SA, Cooper HM. 2006. The Wnt receptor Ryk is required for Wnt5a-mediated axon guidance on the contralateral side of the corpus callosum. J Neurosci 26:5840-5848.

Lesnick TG, Sorenson EJ, Ahlskog JE, Henley JR, Shehadeh L, Papapetropoulos S, Maraganore DM. 2008. Beyond Parkinson disease: amyotrophic lateral sclerosis and the axon guidance pathway. PLoS One 3:e1449.

Li X, Li YH, Yu S, Liu Y. 2008. Upregulation of Ryk expression in rat dorsal root ganglia after peripheral nerve injury. Brain Res Bull 77:178-184.

Lin L, Lesnick TG, Maraganore DM, Isacson O. 2009. Axon guidance and synaptic maintenance: preclinical markers for neurodegenerative disease and therapeutics. Trends Neurosci 32:142-149.

Liu Y, Shi J, Lu CC, Wang ZB, Lyuksyutova AI, Song XJ, Zou Y. 2005. Ryk-mediated Wnt repulsion regulates posterior-directed growth of corticospinal tract. Nat Neurosci 8:1151-1159.

Liu Y, Wang X, Lu CC, Kerman R, Steward O, Xu XM, Zou Y. 2008. Repulsive Wnt signaling inhibits axon regeneration after CNS injury. J Neurosci 28:8376-8382.

Miyashita T, Koda M, Kitajo K, Yamazaki M, Takahashi K, Kikuchi A, Yamashita T. 2009. Wnt-Ryk signaling mediates axon growth inhibition and limits functional recovery after spinal cord injury. J Neurotrauma 26:955-964.

Mulligan VK, Chakrabartty A. 2013. Protein misfolding in the late-onset neurodegenerative diseases: Common themes and the unique case of amyotrophic lateral sclerosis. Proteins.

Nazarenko I, Jenny M, Keil J, Gieseler C, Weisshaupt K, Sehouli J, Legewie S, Herbst L, Weichert W, Darb-Esfahani S, Dietel M, Schafer R, Ueberall F, Sers C. 2010. Atypical protein kinase C zeta exhibits a proapoptotic function in ovarian cancer. Mol Cancer Res 8:919-934.

Nusse R. 2005. Wnt signaling in disease and in development. Cell Res 15:28-32.

Pasinelli P, Brown RH. 2006. Molecular biology of amyotrophic lateral sclerosis: insights from genetics. Nat Rev Neurosci 7:710-723.

Peviani M, Caron I, Pizzasegola C, Gensano F, Tortarolo M, Bendotti C. 2010. Unraveling the complexity of amyotrophic lateral sclerosis: recent advances from the transgenic mutant SOD1 mice. CNS Neurol Disord Drug Targets 9:491-503.

Pratt AJ, Getzoff ED, Perry JJ. 2012. Amyotrophic lateral sclerosis: update and new developments. Degener Neurol Neuromuscul Dis 2012:1-14.

Rosen DR. 1993. Mutations in Cu/Zn superoxide dismutase gene are associated with familial amyotrophic lateral sclerosis. Nature 364:362.

Rosen EY, Wexler EM, Versano R, Coppola G, Gao F, Winden KD, Oldham MC, Martens LH, Zhou P, Farese RV, Jr., Geschwind DH. 2011. Functional genomic analyses identify pathways dysregulated by progranulin deficiency, implicating Wnt signaling. Neuron 71:1030-1042.

Salinas PC, Zou Y. 2008. Wnt signaling in neural circuit assembly. Annu Rev Neurosci 31:339-358.

Schmidt ER, Pasterkamp RJ, van den Berg LH. 2009. Axon guidance proteins: novel therapeutic targets for ALS? Prog Neurobiol 88:286-301.

Schmitt AM, Shi J, Wolf AM, Lu CC, King LA, Zou Y. 2006. Wnt-Ryk signalling mediates medial-lateral retinotectal topographic mapping. Nature 439:31-37.

Shao CY, Crary JF, Rao C, Sacktor TC, Mirra SS. 2006. Atypical protein kinase C in neurodegenerative disease II: PKCiota/lambda in tauopathies and alpha-synucleinopathies. J Neuropathol Exp Neurol 65:327-335.

Valentine JS, Doucette PA, Zittin Potter S. 2005. Copper-zinc superoxide dismutase and amyotrophic lateral sclerosis. Annu Rev Biochem 74:563-593.

Vanderhaeghen P, Cheng HJ. 2010. Guidance molecules in axon pruning and cell death. Cold Spring Harb Perspect Biol 2:a001859.

Wang G, Silva J, Krishnamurthy K, Tran E, Condie BG, Bieberich E. 2005. Direct binding to ceramide activates protein kinase Czeta before the formation of a pro-apoptotic complex with PAR-4 in differentiating stem cells. J Biol Chem 280:26415-26424.

Wang S, Guan Y, Chen Y, Li X, Zhang C, Yu L, Zhou F, Wang X. 2013. Role of Wnt1 and Fzd1 in the spinal cord pathogenesis of amyotrophic lateral sclerosis-transgenic mice. Biotechnol Lett.

Wolf AM, Lyuksyutova AI, Fenstermaker AG, Shafer B; Lo CG; Zou Y. 2008. Phosphatidylinositol-3-kinase-atypical protein kinase C signaling is required for Wnt attraction and anterior-posterior axon guidance. Journal of Neuroscience 28(13):3456-3467.

Wooten MW. 1999. Function for NF-kB in neuronal survival: regulation by atypical protein kinase C. J Neurosci Res 58:607-611.

Wooten MW, Seibenhener ML, Neidigh KB, Vandenplas ML. 2000. Mapping of atypical protein kinase C within the nerve growth factor signaling cascade: relationship to differentiation and survival of PC12 cells. Mol Cell Biol 20:4494-4504.

Xie J, Guo Q, Zhu H, Wooten MW, Mattson MP. 2000. Protein kinase C iota protects neural cells against apoptosis induced by amyloid beta-peptide. Brain Res Mol Brain Res 82:107-113.

Xin M, Gao F, May WS, Flagg T, Deng X. 2007. Protein kinase Czeta abrogates the proapoptotic function of Bax through phosphorylation. J Biol Chem 282:21268-21277.

Yu L, Guan Y, Wu X, Chen Y, Liu Z, Du H, Wang X. 2013. Wnt Signaling is Altered by Spinal Cord Neuronal Dysfunction in Amyotrophic Lateral Sclerosis Transgenic Mice. Neurochem Res.

Zhang X, Zhu J, Yang GY, Wang QJ, Qian L, Chen YM, Chen F, Tao Y, Hu HS, Wang T, Luo ZG. 2007. Dishevelled promotes axon differentiation by regulating atypical protein kinase C. Nat Cell Biol 9:743-754.

Zou Y. 2004. Wnt signaling in axon guidance. Trends Neurosci 27:528-532.

FIGURE LEGENDS

Figure 1: **aPKC and Ryk are expressed in ChAT$^+$ motor neurons and CC1$^+$ oligodendrocytes in the adult ventral spinal cord.** Immunostaining of coronal sections of lumbar spinal cords of 60 day-old mice for aPKC (**A-C**) or Ryk (**E-G**), Neurofilament 200 (NF-200) marker or astrocyte marker GFAP or postmitotic oligodendrocyte CC1 marker and motor neuron marker ChAT. aPKC and Ryk are not expressed in GFAP$^+$ cells (B,F). Arrows in A-C and E-G indicate neurons double labeled for aPKC or Ryk and ChAT. Arrowheads in A indicate aPKC$^+$ NF-200$^+$ ChAT$^-$ neurons. Arrowheads in C indicate aPKC$^+$ CC1$^+$ cells. Arrowheads in E indicate colocalization of Ryk with ChAT immunostaining in motor axons in the ventral white matter. Arrowheads in G indicate Ryk$^+$ CC1$^+$ cells. D and H are higher magnifications showing the intracellular localization of aPKC and Ryk immunoreactivity. aPKC immunoreactivity is localized in both cytoplasm and nucleus (arrowheads in D). Ryk immunoreactivity is mainly localized in the cytoplasm of motor neuron cell bodies (arrows in H) and in fibers (arrowheads in H). Scale bars: 100 µm (A-C, E-G), 50 µm (D,H).

Figure 2: **aPKC expression is increased in the motor neurons of the ventral lumbar spinal cord of SOD1 (G93A) mice**. Immunostaining of coronal sections of lumbar spinal cords of non transgenic (NT), SOD1 (WT) and SOD1 (G93A) mice of 30, 60, 90 and 120 days for aPKC (green) and ChAT (red). **A**, Representative pictures of aPKC/ChAT double immunostaining in P30 NT, SOD1(WT) and SOD1 (G93A) lumbar spinal cords. Arrows indicate motor neurons double labeled for aPKC and ChAT. **B**, Quantification of aPKC immunoreactivity in ChAT+ motor neurons (MN) in the ventral lumbar spinal cord at different stages of symptom progression. **C**, Mean number of ChAT$^+$ MN counted per section at different stages. Data represent mean±SEM, n=3-10 animals/group, ** P<0.01, ANOVA with Bonferroni Post-test. Scale bar: 50 µm.

Figure 3: **aPKC is colocalized with human SOD1 in extracellular aggregates**. Immunostaining of coronal sections of lumbar spinal cords of non transgenic (NT), SOD1 (WT) and SOD1 (G93A) mice of 120 days for aPKC (green), human SOD1 (red) and ChAT (blue). **A**, aPKC colocalizes with human SOD1 in the lumbar spinal cord of P120 SOD1 (G93A) mice (arrows). **B**, Higher magnifications showing colocalization of aPKC with human SOD1 protein in $ChAT^+$ motor neurons (arrows) and in extracellular aggregates (arrowheads) in the ventral lumbar spinal cord of P120 SOD1-G93A mice. **C**, Quantification of the number of aPKC aggregates per section in NT, SOD1 (WT) and SOD1 (G93A) mice at different stages. Data represent mean±SEM, n=3-5 animals/group, ** $p<0.01$, *** $p<0.001$, ANOVA with Bonferroni Post-test. Scale bars: 50 µm (A, C), 25 µm (B).

Figure 4: **aPKC is enriched in the detergent-insoluble fraction but decreased in the detergent-soluble fraction**. **A,** Western-blottings with protein lysates from detergent-soluble (S) and insoluble fractions (I) of non transgenic (NT) and SOD1 (G93A) lumbar spinal cords at P120. The graph represents the ratio of aPKC protein level in the insoluble fraction over the soluble fraction, the I/S ratio being set at 1 in the NT mouse group (n=3 animals/group). **B,** Western-blotting with protein lysates from detergent-soluble fractions of NT and SOD1 (G93A) lumbar spinal cords at P30 and P90 (n=3-5 animals/group).* $p<0.05$, Student's t test.

Figure 5: Ryk expression is increased in the motor neurons and the white matter of the ventral lumbar spinal cord of SOD1-G93A mice. Immunostaining of coronal sections of lumbar spinal cords of non transgenic (NT), SOD1 (WT) and SOD1 (G93A) mice of 30, 60, 90 and 120 days for Ryk (green) and ChAT (red). **A**, Representative pictures of Ryk/ChAT double immunostaining in P30 NT, SOD1 (WT) and SOD1 (G93A) lumbar spinal cords. Arrows indicate motor neurons double labeled for Ryk and ChAT. **B**, Quantification of Ryk immunoreactivity in

ChAT$^+$ motor neurons (MN) in the ventral lumbar spinal cord at different stages. **C**, Ryk immunostaining in the white matter of the ventral lumbar spinal cord of P120 NT, SOD1 (WT) and SOD1 (G93A) mice. Arrows indicate increased Ryk immunoreactivity in the ventral white matter of SOD1 (G93A) mice. **D,** Quantification of Ryk immunoreactivity in the ventral white matter of lumbar spinal cord of NT, SOD1 (WT) and SOD1 (G93A) mice at different stages. **E**, Colocalization of Ryk with NF-200 in the white matter of the ventral spinal cord of P120 SOD1 (G93A) mice. **F**, Ryk is expressed in SMI-312$^+$ axons in the ventral roots of P120 SOD1 (G93A) mice. Data represent mean±SEM, n=3-10 animals/group, * $p<0.05$, ** $p<0.01$, *** $p<0.001$, ANOVA with Bonferroni Post-test. Scales bars: 50 µm (A,C,E,F).

Figure 6: **Ryk is colocalized with human SOD1 protein in motor neurons and in the white matter of SOD1-G93A mouse lumbar spinal cord but not in extracellular aggregates**. **A**, Immunostaining of coronal sections of lumbar spinal cords of P120 SOD1 (G93A) mice for Ryk (green), human SOD1 (red) and ChAT (blue). Ryk is colocalized with human SOD1 protein in ChAT$^+$ motor neurons (arrows) in the ventral lumbar spinal cord of P120 SOD1 (G93A) mice. **B**, Colocalization of Ryk expression with human SOD1 protein in the white matter of the ventral spinal cord of P120 SOD1 (G93A mice). Scales bars: 25 µm (A), 100 µm (B).

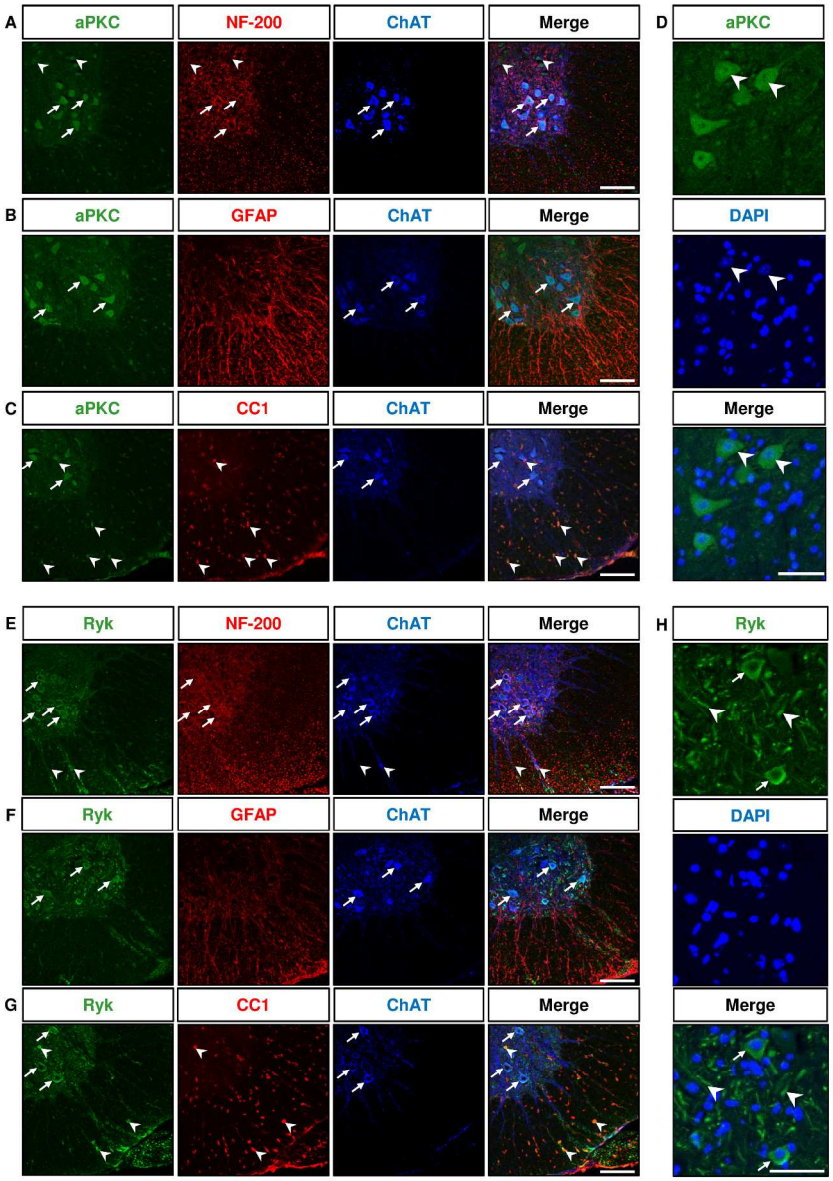

250x354mm (300 x 300 DPI)

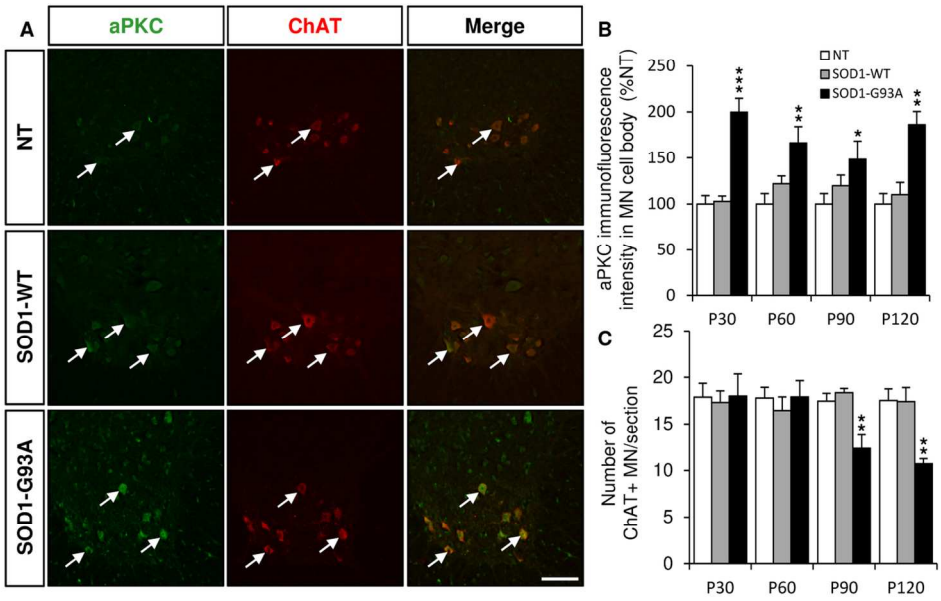

123x80mm (300 x 300 DPI)

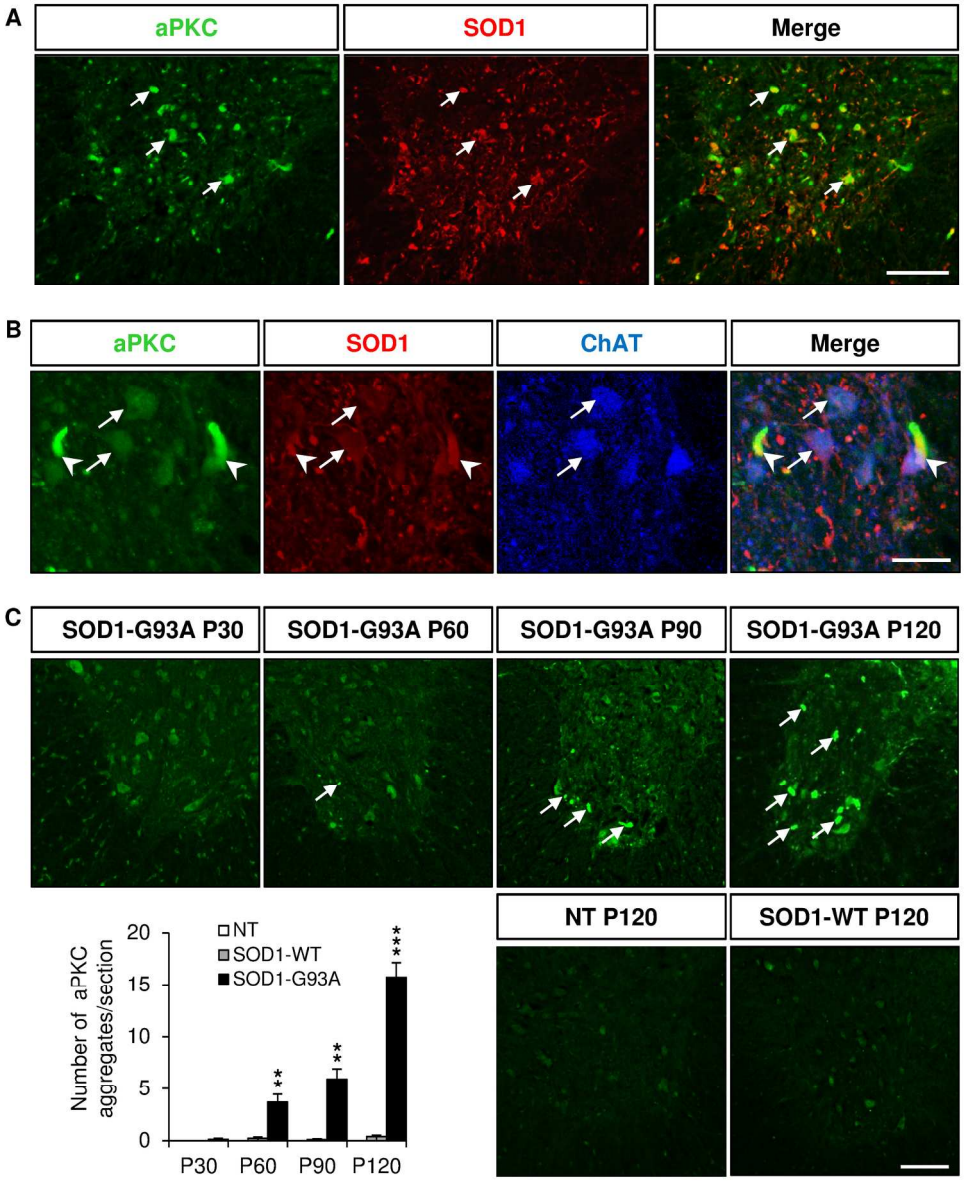

197x237mm (300 x 300 DPI)

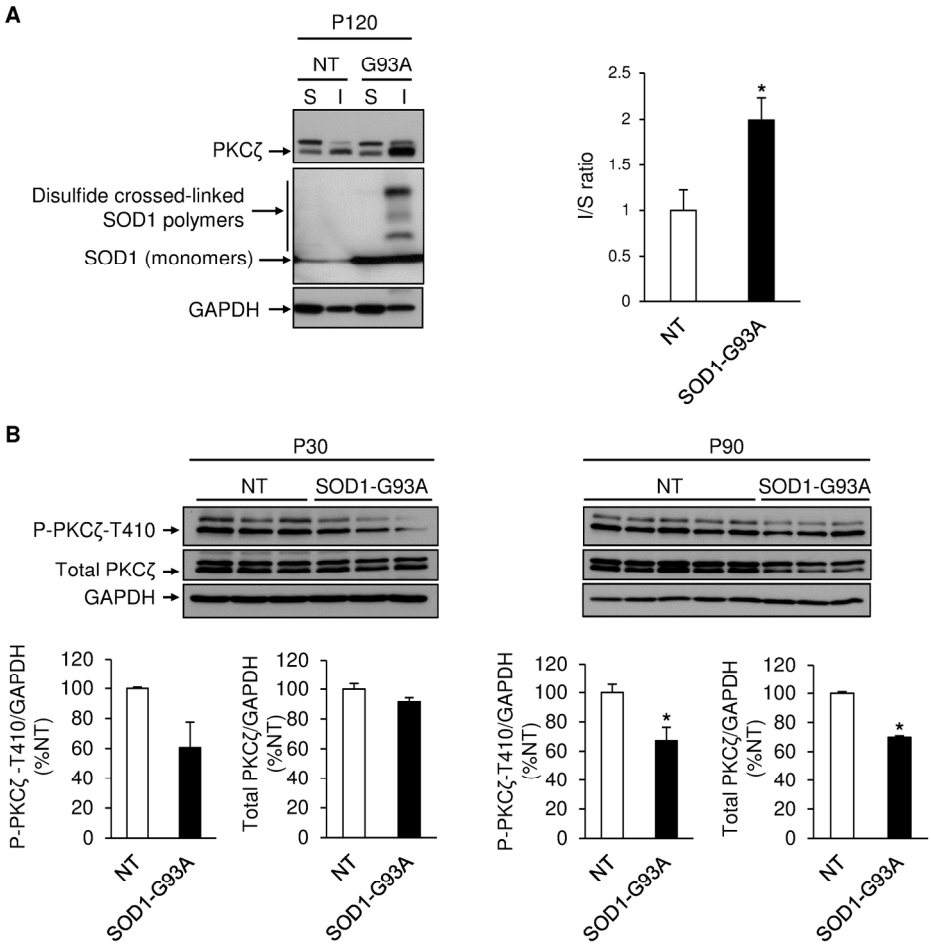

179x183mm (300 x 300 DPI)

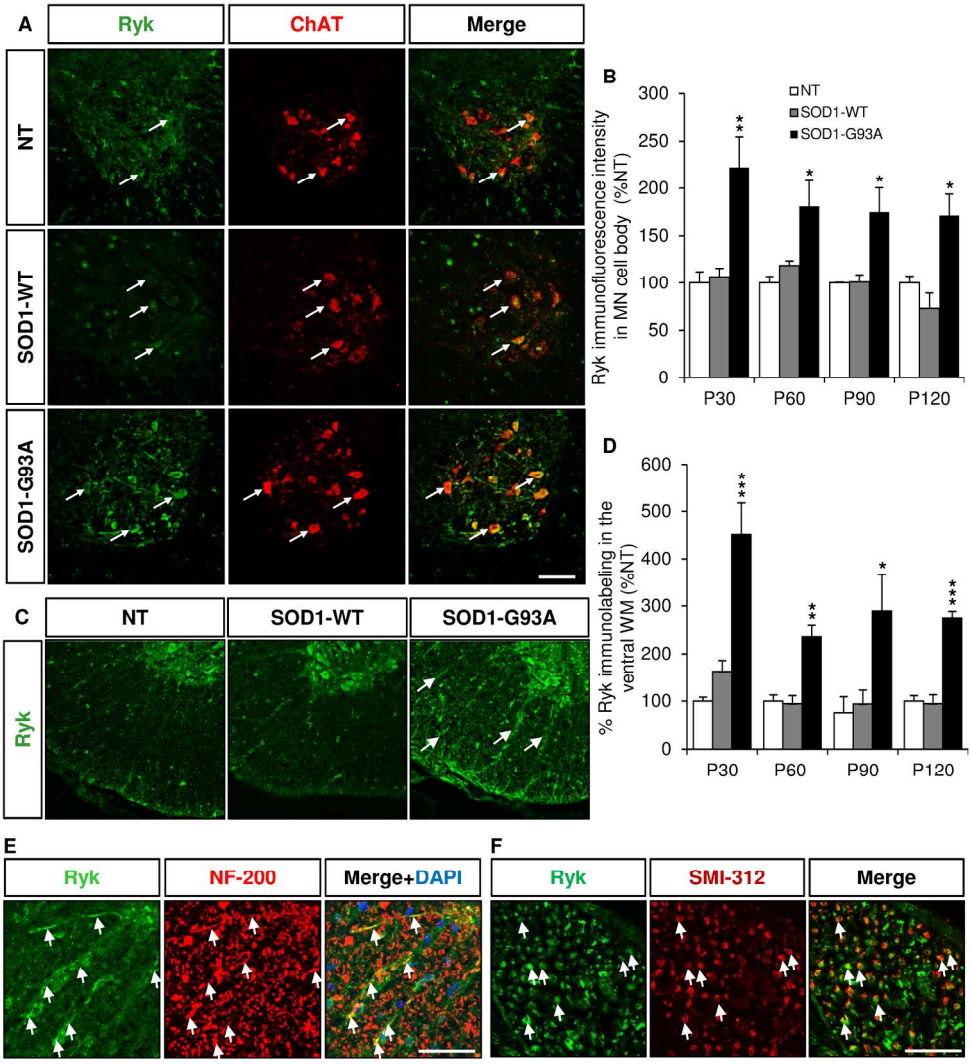

209x226mm (300 x 300 DPI)

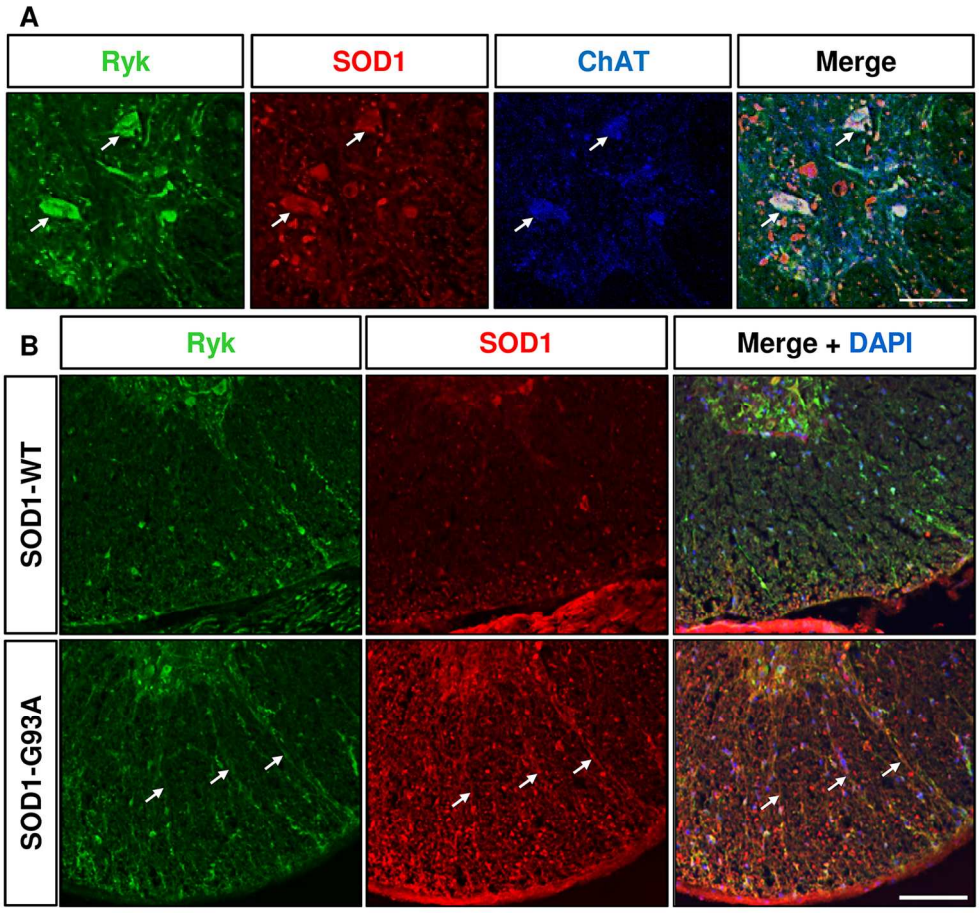

141x132mm (300 x 300 DPI)